THE JOURNAL OF PHYSICAL CHEMISTRY B

Article

Pyrazine in Supercritical Xenon: Local Number Density Defined by Experiment and Calculation

Bruce J. Hrnjez, Abdo Kabarriti, Benjamin I. Dach, Sergey V. Buldyrev, Neer Asherie, Georgiy R. Natanov, and Joshua Balderman

J. Phys. Chem. B, **2008**, 112 (48), 15431-15441• DOI: 10.1021/jp807586d • Publication Date (Web): 07 November 2008

Pyrazine in Supercritical Xenon: Local Number Density Defined by Experiment and Calculation

Bruce J. Hrnjez,*,† Abdo Kabarriti,† Benjamin I. Dach,† Sergey V. Buldyrev,‡ Neer Asherie,‡,§ Georgiy R. Natanov,† and Joshua Balderman†

Departments of Chemistry, Physics, and Biology, Yeshiva University, New York, New York 10033

Received: August 25, 2008; Revised Manuscript Received: September 22, 2008

Toward our goal of using supercritical fluids to study solvent effects in physical and chemical phenomena, we develop a method to spatially define the solvent local number density at the solute in the highly compressible regime of a supercritical fluid. Experimentally, the red shift of the pyrazine n$-\pi^*$ electronic transition was measured at high dilution in supercritical xenon as a function of pressure from 0 to ~24 MPa at two temperatures: one (293.2 K) close to the critical temperature and the other (333.2 K) remote. Computationally, several representative stationary points were located on the potential surfaces for pyrazine and 1, 2, 3, and 4 xenons at the MP2/6-311++G(d,p)/aug-cc-pVTZ-PP level. The vertical n$-\pi^*$ ($^1B_{3u}$) transition energies were computed for these geometries using a TDDFT/B3LYP/DGDZVP method. The combination of experiment and quantum chemical computation allows prediction of supercritical xenon bulk densities at which the pyrazine primary solvation shell contains an *average* of 1, 2, 3, and 4 xenon molecules. These density predictions were achieved by graphical superposition of calculated shifts on the experimental shift versus density curves for 293.2 and 333.2 K. Predicted bulk densities are 0.50, 0.91, 1.85, and 2.50 g cm^{-3} for average pyrazine primary solvation shell occupancy by 1, 2, 3, and 4 xenons at 293.2 K. Predicted bulk densities are 0.65, 1.20, 1.85, and 2.50 g cm^{-3} for average pyrazine primary solvation shell occupancy by 1, 2, 3, and 4 xenons at 333.2 K. These predictions were evaluated with classical Lennard-Jones molecular dynamics simulations designed to replicate experimental conditions at the two temperatures. The average xenon number within 5.0 Å of the pyrazine center-of-mass at the predicted densities is 1.3, 2.1, 3.0, and 4.0 at both simulation temperatures. Our three-component method—absorbance measurement, quantum chemical prediction, and evaluation of prediction with classical molecular dynamics simulation—therefore has a high degree of internal consistency for a system in which the intermolecular interactions are dominated by dispersion forces.

Introduction

Supercritical fluids may be viewed as tools that will allow us to study solvent effects without changing the solvent.[1,2] The traditional approach to the study of solvent effects, in which the solvent is changed and the response of the system is measured,[3] involves far more than a mere change in bulk solvent properties; it necessarily involves a change in the discrete interactions between solute and solvent molecules. All traditional studies of solvent effects are therefore complicated by the many variables that change simultaneously. The use of supercritical fluids as tools to study solvent effects allows us to circumvent the multivariable problem that unavoidably accompanies a solvent change.

In a supercritical fluid, a chemical or physical process can be studied in the fluid of interest at constant temperature above the critical temperature (T_C) as a function of pressure and, therefore, density of the medium. Operation above T_C precludes the complication of a gas−liquid phase change, and the density of the medium can be varied continuously from gas-like to liquid-like. Bulk solvent properties such as dielectric constant, refractive index, and viscosity vary predictably with density, while the types of intermolecular interactions available to solute and solvent remain constant. We can therefore study solvent effects without changing the solvent.

A complication we must resolve is that the local solvent number density in the immediate vicinity of a solute and the bulk solvent number density are usually not equal in the low to medium bulk density regime of a supercritical fluid at temperatures close to the critical. This well-studied and thoroughly reviewed disparity[4−9] arises when the attractive interaction energy between a given solute−solvent pair (ε_{ij}) is greater (most commonly) than that between the solvent−solvent pair (ε_{jj}) such that $|\varepsilon_{ij} - \varepsilon_{jj}|/k_BT > 1$. Under these circumstances, the solvent clusters about the solute and the local solvent number density is higher than the bulk solvent number density. When the solvent number density in the solute primary solvation sphere cannot be approximated by the bulk solvent number density, the local solvent property values are not the same as the measurable and calculable bulk values. We contend that this disparity is not yet adequately defined, particularly in its three-dimensional details; this lack of definition compromises our ability to use supercritical fluids to understand solvent effects. We therefore work toward a better practical understanding of this clustering phenomenon, sometimes known as local density augmentation or enhancement,[4] in the highly compressible regime of supercritical fluids.

The system is pyrazine in xenon. Pyrazine (see Figure 1) is well-known to the computational and spectroscopic communities,[10−15] and the pyrazine−one xenon cluster produced by

* Corresponding author: Tel 212-960-5444, e-mail hrnjez@yu.edu.
† Department of Chemistry.
‡ Department of Physics.
§ Department of Biology.

10.1021/jp807586d CCC: $40.75
Published on Web 11/08/2008

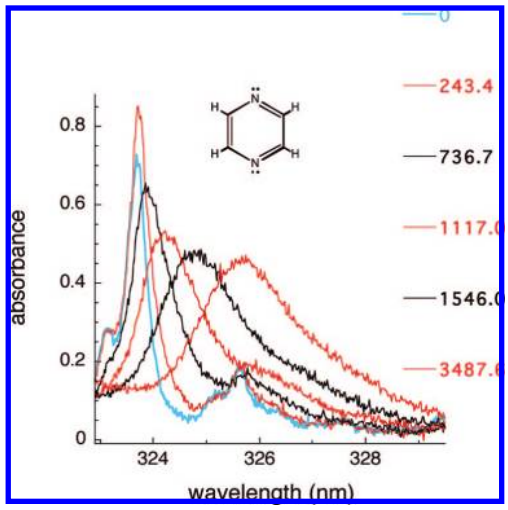

Figure 1. The 0−0 absorbance band of the pyrazine n−π* transition at 333.2 K and representative xenon pressures, ranging from 0 to 3316.8 psia (0−22.87 MPa). Shown also is the structure of pyrazine with its two in-plane lone pairs.

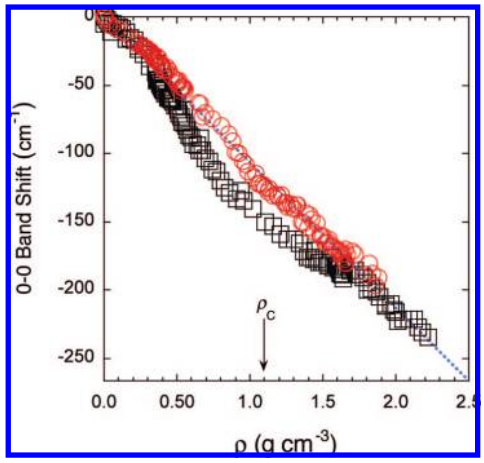

Figure 2. Red shift of 0−0 band maximum of pyrazine n−π* transition as a function of xenon bulk density from 0 to about 24.1 MPa at 293.2 K (black open squares) and 333.2 K (red open circles).

supersonic expansion has been examined by two-color double-resonance spectroscopy.[16] Holroyd studied electron attachment to pyrazine in supercritical xenon.[17] The highly polarizable xenon[18] is a simple model for hydrocarbon solvation, and its spherical symmetry conveniently limits the orientational degrees of freedom with respect to the pyrazine solute. The pyrazine−xenon system is conceptually simplified by the fact that dispersion forces dominate the intermolecular interactions.

The experimental and computational model is the pyrazine n−π* electronic transition in supercritical xenon (T_C = 289.74 K, P_C = 5.842 MPa, ρ_C = 8.371 mol L^{-1} = 1.099 g cm^{-3}),[19,20] studied as a function of density at two temperatures: one close to and the other remote from T_C. We report (1) the experimental UV absorbance behavior of the supercritical xenon−pyrazine system, (2) the quantum chemically determined representative structures for pyrazine and 1, 2, 3, and 4 xenons, (3) the computed n−π* transition energies of these structures, (4) a computational probe of the pyrazine−xenon potential surface designed to reveal the n−π* transition energy sensitivity to xenon movement on this potential surface, (5) our prediction of the supercritical xenon bulk densities at which the pyrazine primary solvation sphere contains an average of 1, 2, 3, and 4 xenons, and (6) a test of our predictions with classical molecular dynamics simulations of pyrazine in supercritical xenon. If experiment, computational prediction, and computational test of prediction are internally consistent, the primary solvation sphere at the pyrazine solute may be considered characterized. This characterization is the minimum requirement for using the supercritical medium as a tool to understand solvent effects.

Experimental Methods

The experiments were performed as described previously in detail.[1] Briefly, absorbance measurements were made with a Cary 300 UV−vis spectrophotometer with a limiting resolution rated to less than 0.2 nm. Routine data collection with a 0.2 nm slit width and 0.02 nm data intervals focused on the 0−0 band of the pyrazine n−π* transition in the region 335−322 nm (29 851−31 056 cm^{-1}). The absorbance maximum for the gas phase 0−0 band was reproducibly 323.78 ± 0.02 nm (30 885.2 cm^{-1}, literature value 323.88 nm, 30 875.6 cm^{-1})[14,15] at about 30 mTorr. Experiments were conducted at constant temperature (293.2 or 333.2 ± 0.1 K) as a function of pressure from 0 to ~24 ± 0.01 MPa at pressure intervals as small as 0.03 MPa in the highly compressible regime. The pressure was manipulated with a syringe pump. Each of the two reported data sets (293.2 and 333.2 K) is a composite of several data sets. Bulk xenon densities (±0.2%) were calculated online with an equation of state[19] used for calculation of fluid properties by the National Institute of Standards and Technology (NIST) Chemistry WebBook service.[20]

Pyrazine (>99%) was purchased from Aldrich Chemical Co. and used without further purification. Pyrazine readily sublimes at room temperature and atmospheric pressure; we therefore used material that had sublimed to the upper walls of the storage bottle. Xenon (99.999%) was purchased from TechAir (White Plains, NY) and used without further purification. The UV spectrum of xenon at high density did not reveal contamination by any UV-absorbing substances in the region of interest. Pyrazine was loaded reproducibly as before[1] to give a constant pyrazine concentration of about 1.6 × 10^{-6} M over the course of a single data collection run at constant temperature as a function of incremental addition of xenon (increasing pressure at constant vessel volume).

Computational Methods

Ab initio electronic structure calculations for pyrazine, xenon, xenon dimer, and pyrazine with 1, 2, 3, and 4 xenons were performed with Gamess,[21,22] PC Gamess,[23] and Gaussian03.[24] Stationary points were located on the potential surfaces for pyrazine and 1, 2, 3, and 4 xenons at a modest level of quantum chemical theory, using the second-order Møller−Plesset perturbation[25] (MP2) method, the 6-311++G(d,p)[26] medium-sized basis set for C, H, and N, and the aug-cc-pVTZ-PP basis set with an effective core potential (28 electron ECP28MDF) for xenon.[27] Vertical n−π* ($^1B_{3u}$) transition energies[10] were computed with a time-dependent density functional[28] (TDDFT) method using the hybrid Becke-style three-parameter density functional theory (DFT) with the Lee−Yang−Parr correlation functional[29] (B3LYP) and the modestly sized DZVP[11] (DGDZ-VP within the program package Gaussian 03) basis set. Program package defaults, including criteria for wave function convergence and locations of stationary points on potential surfaces, were used. Geometry optimizations for configurations of pyrazine with 1, 2, 3, and 4 xenons were performed without incorporation of the counterpoise method[31] into the optimization routine. For estimation of the basis set superposition error (BSSE), the counterpoise method was applied to optimized

TABLE 1: Calculated Ground State MP2/6-311++G(d,p)/aug-cc-pVTZ-PP Energies and Excited State TDDFT/B3LYP/DGDZVP Singlet n−π* Transition Energies for Pyrazine and 1, 2, 3, and 4 Xenons

system	$E_{electronic}$ (au)	$E_{corrected}$[a] (au)	E_b[b] (kcal)	n−π* (nm)	n−π* (cm^{-1})	calculated shift[c] (cm^{-1})	average shift[d] (cm^{-1})
pyrazine	−263.6308815			311.30	32123.4	0	0
one xenon	−328.5491126						
two xenons	−657.0998564	−657.0990768	−0.53				
1	−592.1853480	−592.1827693	−1.74	311.88	32063.6	−59.8	−52.8
2a	−920.7403850	−920.7347073	−3.51	312.84	31965.2	−158.3	−142.1
2b	−920.7390384	−920.7336849	−2.87	312.23	32027.7	−95.7	
2c	−920.7391826	−920.7336837	−2.87	312.88	31961.1	−162.2	
2d	−920.7394372	−920.7338540	−2.99	312.51	31999.0	−124.4	
3a	−1249.2945297	−1249.2856892	−4.69	313.54	31893.9	−229.5	−225.1
3b	−1249.2942655	−1249.2855262	−4.58	313.96	31851.2	−272.2	
3c	−1249.2941056	−1249.2855436	−4.60	313.00	31948.9	−174.4	
4a	−1577.8480597	−1577.8365917	−5.81	314.82	31764.2	−359.2	−249.2
4b	−1577.8477166	−1577.8366988	−5.88	312.70	31979.5	−143.8	
4c	−1577.8485738	−1577.8369664	−6.04	313.81	31866.4	−256.9	

[a] Counterpoise-corrected energy. [b] Cluster binding energy (mol^{-1}) relative to isolated pyrazine and xenon. [c] With respect to isolated pyrazine table entry (32 123.4 cm^{-1}). [d] The average shift for **1** is the Boltzmann-weighted average (T = 293.15 K) for all configurations explored on the potential surface defined in Figures 7−9. The average shifts for **2**, **3**, and **4** are the Boltzmann-weighted averages for the configurations reported in this table. The values changed insignificantly when calculated at 333.15 K.

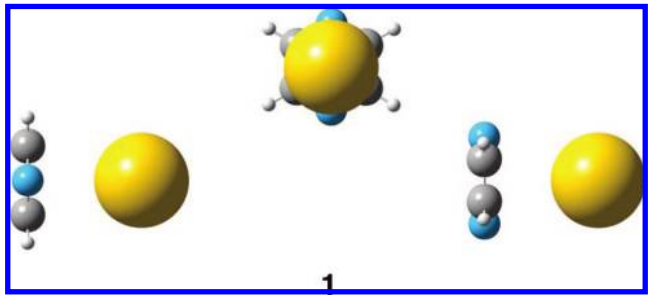

Figure 3. Structure **1** for pyrazine and one xenon. Blue is nitrogen, gray is carbon, white is hydrogen, and yellow is xenon, all scaled to 75% of their van der Waals radii. Three perspectives are shown: left structure has pyrazine plane and N−N axis perpendicular to page; middle structure has pyrazine plane coplanar with page; right structure has pyrazine plane perpendicular to page and N−N axis coplanar with page.

structures. Two geometry optimizations incorporating the counterpoise method[32,33] (readily accomplished with Gaussian 03) and with different basis sets were performed for our configuration in which pyrazine and one xenon are most strongly bound: MP2/6-311++G(d,p)/aug-cc-pVTZ-PP (215 basis functions) and MP2/aug-cc-pVTZ-PP (423 basis functions).[34−39] Single-point, counterpoise-corrected energies at the MP2/aug-cc-pVQZ-PP (968 basis functions)[40] level were calculated for both of these structures.

Equilibrium molecular dynamics simulations[41,42] of pyrazine in xenon were performed with the GROMACS program package.[43] Nonbonded interactions were modeled with eq 1, a standard Lennard-Jones potential, $\phi_{LJ}(r_{ij})$, in which the atoms *i, j* are treated as hard spheres separated by distance *r* with well depth ε and governed by the combination rules in eqs 2 and 3.

$$\phi_{LJ}(r_{ij}) = 4\varepsilon_{ij}\left[\left(\frac{\sigma_{ij}}{r_{ij}}\right)^{12} - \left(\frac{\sigma_{ij}}{r_{ij}}\right)^{6}\right] \quad (1)$$

$$\varepsilon_{ij} = (\varepsilon_{ii}\varepsilon_{jj})^{1/2} \quad (2)$$

$$\sigma_{ij} = (\sigma_{ii}\sigma_{jj})^{1/2} \quad (3)$$

We chose to use the Lennard-Jones xenon parameters given by Egorov,[44] ε/k_B = 220.8 K (well depth 0.44 kcal/mol) and σ = 3.96 Å, and a cutoff of 20.0 Å (5.05σ), to which long-range dispersion corrections were applied. The pyrazine topology file was created on the Dundee PRODRG2 Server[45,46] using pyrazine coordinates obtained from a quantum chemical geometry optimization at the MP2/6-311++G(d,p) level. We used the recommended Gromos96 united-atom force field[43] and the SHAKE constraint algorithm to fix pyrazine geometry. Cubic periodic boxes containing 1000 xenon atoms and one pyrazine molecule were temperature-coupled with the Berendsen thermostat, but not pressure-coupled to a barostat. Box side lengths ranged from 200 to 44.4 Å, affording a bulk density range of

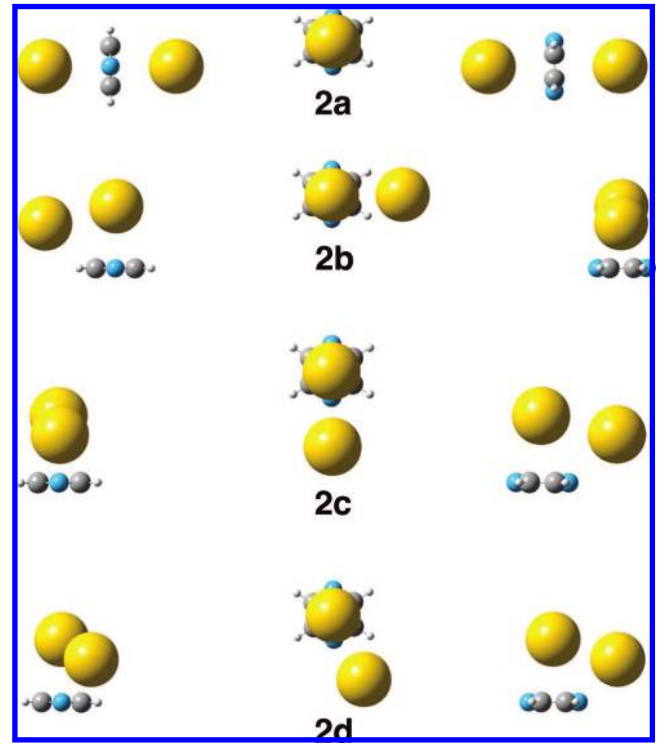

Figure 4. Structures **2a**−**d** for pyrazine and two xenons. Blue is nitrogen, gray is carbon, white is hydrogen, and yellow is xenon, all scaled to 75% of their van der Waals radii. Three perspectives are shown: left column structures have pyrazine plane and N−N axis perpendicular to page; middle column structures have pyrazine plane coplanar with page; right column structures have pyrazine plane perpendicular to page and N−N axis coplanar with page.

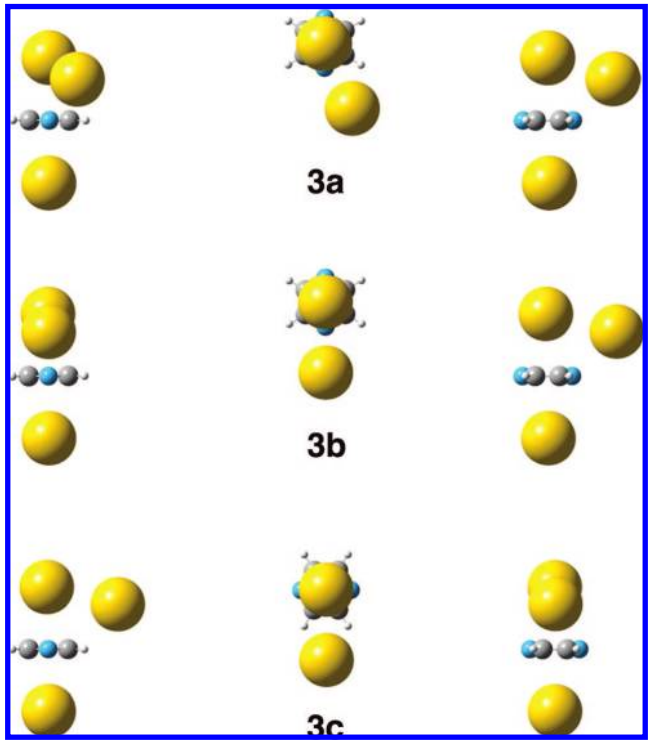

Figure 5. Structures **3a**−**c** for pyrazine and three xenons. Blue is nitrogen, gray is carbon, white is hydrogen, and yellow is xenon, all scaled to 75% of their van der Waals radii. Three perspectives are shown: left column structures have pyrazine plane and N−N axis perpendicular to page; middle column structures have pyrazine plane coplanar with page; right column structures have pyrazine plane perpendicular to page and N−N axis coplanar with page.

0.027−2.50 g cm^{-3}. Under these simulation conditions, the xenon critical temperature is 293.5 K, which is within about 1% of the experimental value. The simulation temperatures were 296.9 K (T_C + 3.4 K) and 336.9 K (T_C + 43.4 K). Time steps of 2 fs for 10 million steps gave a total simulation time of 20 ns. Integration of the equations of motion was performed according to a leapfrog method in GROMACS.

Results and Discussion

Our ultimate objective is to use supercritical fluids as tools to study solvent effects on physical and chemical phenomena; our present objective is to achieve a three-dimensional understanding of the local environment of pyrazine in xenon. This study has three components. The first component is the experimental description of how pyrazine absorbs UV light as a function of xenon bulk density. The second component is the quantum chemical description of the ground-state potential surface of pyrazine and 1, 2, 3, and 4 xenons and of how pyrazine absorbs UV light as a function of xenon number and orientation with respect to pyrazine. These two components should allow prediction of the experimental densities at which pyrazine is associated with an *average* of 1, 2, 3, and 4 xenons. The third component is the classical molecular dynamics description of local xenon number density at the solute pyrazine as a function of bulk density. These molecular dynamics simulations allow us to evaluate the integrity of our density predictions and to acquire insight into the width of xenon number distribution in the pyrazine primary solvation sphere at a given bulk density.

Pyrazine in Supercritical Xenon. Operation above T_C affords continuous variation in bulk fluid density from gas-like to liquid-like values and excludes the complication of gas−liquid phase transitions. We begin with pyrazine at very low concentration in the absence of xenon. Our vibrationally well-resolved spectrum of the gas phase n−π^* transition for pyrazine is previously reported.[1] The principal features of this spectrum remain resolved even at the highest xenon density studied (ca. 2.2 g cm^{-3}) and shift to the red with increasing xenon density. We focused on the 0−0 band at 30 885.2 cm^{-1} (323.78 nm). Figure 1 shows the typical behavior of this band at 333.2 K and representative pressures from 0 (<30 mTorr in pyrazine) to 22.87 MPa. (The behavior at 293.2 K, not shown, is qualitatively similar.) The integrated area of the 323.78 nm band origin at 0 psia increases with the introduction of xenon. The band broadens and the area increases with density. The total red shift is −206.6 cm^{-1} at 293.2 K (T_C + 3.4 K) and −191.0 cm^{-1} at 333.2 K (T_C + 43.4 K), which correspond to a decrease in the n−π^* transition energy of 0.65 and 0.55 kcal mol^{-1}, respectively.

The observed band area increase may correspond to a local xenon refractive index effect on the pyrazine n−π^* transition oscillator strength. Meyers and Birge derived a simple expression to account for their experimental observations with pyrazine and a series of hydrocarbon solvents; it requires knowledge of the solvent refractive index and a geometric factor that depends on the shape of the solute and the orientation of its transition moment.[47,48] We recently presented[49] a preliminary comparison of experiment and theory, in which we evaluated the theoretical prediction that the sign and magnitude of the change in solute excitation oscillator strength depends on the change in solvent refractive index and the shape of the solute approximated as a cylinder.

The experimental data translated to 0−0 band shift in wavenumbers with respect to density at both 293.2 and 333.2

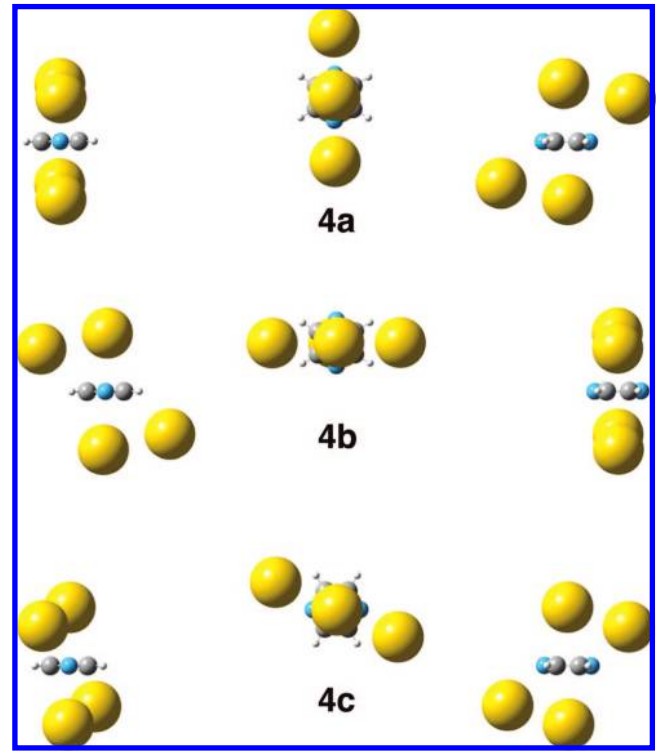

Figure 6. Structures **4a**−**c** for pyrazine and four xenons. Blue is nitrogen, gray is carbon, white is hydrogen, and yellow is xenon, all scaled to 75% of their van der Waals radii. Three perspectives are shown: left column structures have pyrazine plane and N−N axis perpendicular to page; middle column structures have pyrazine plane coplanar with page; right column structures have pyrazine plane perpendicular to page and N−N axis coplanar with page.

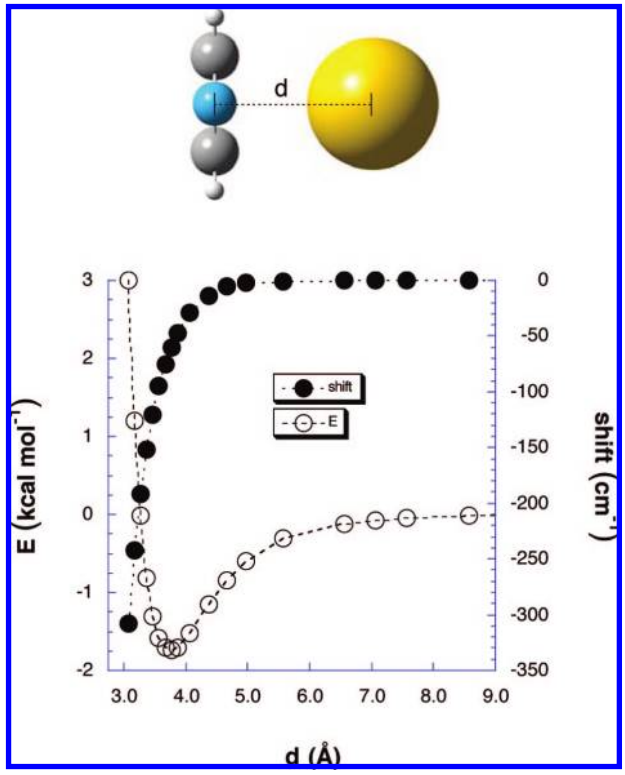

Figure 7. Energy and calculated n−π* shift of **1** as a function of pyrazine−xenon distance. The distance coordinate (d) is a line perpendicular to the pyrazine plane and passing though the pyrazine center of mass. Open circles indicate energy as a function of intermolecular distance. Filled circles indicate shift in calculated n−π* transition relative to isolated pyrazine as a function of intermolecular distance.

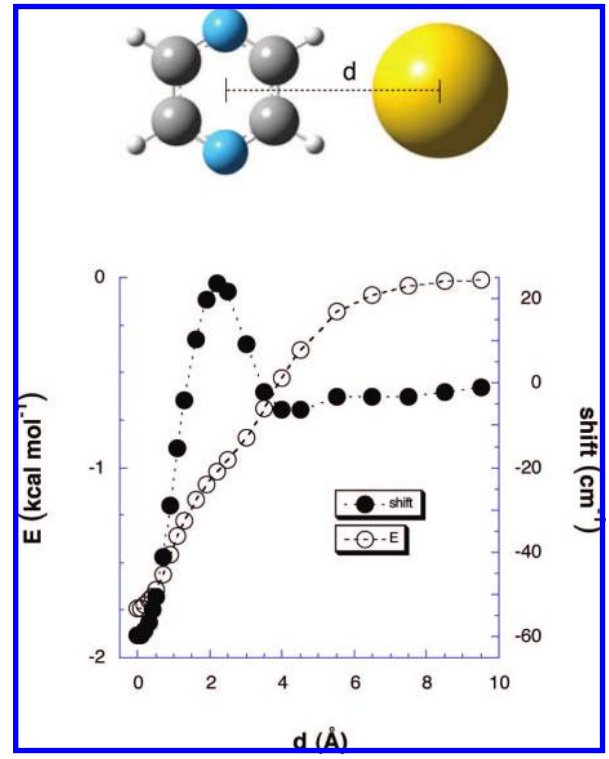

Figure 8. Energy and calculated n−π* shift of **1** as a function of xenon movement in the plane above pyrazine. Zero on the distance coordinate (d) corresponds to the potential minimum for the system. The distance coordinate is a line parallel to and 3.772 Å from the pyrazine plane. Open circles indicate the CP-corrected energy of the system as a function of distance. Filled circles indicate shift in calculated n−π* transition relative to isolated pyrazine for each of these configurations.

K is shown in Figure 2. The dashed line, defined by the apparently linear regions at low and high densities, represents the expected behavior of the system if the local xenon density at pyrazine were equal to the bulk xenon density. The local xenon number density at pyrazine is greater than the bulk number density from about 0.2 to 1.7 g cm^{-3} at 293.2 K and accounts for the observed deviation from linearity. The almost linear behavior at the higher temperature suggests that the bulk and local xenon number density are nearly equal at 333.2 K; higher temperature diminishes the importance of the relatively small potential difference between the pyrazine−xenon and xenon−xenon systems.

Pyrazine and Xenon Computational Approach. Pyrazine's primary solvation sphere must fill stepwise with an *average* of 1, 2, 3, and 4 xenons with increasing density. Geometry optimization gave representative structures **1**, **2a**−**d**, **3a**−**c**, and **4a**−**c** for pyrazine and 1, 2, 3, and 4 xenons (Figures 3−6 and Table 1). Regardless of starting configuration, all geometry optimizations of pyrazine and one xenon led to **1** (Figure 3), in which the xenon is centered above the pyrazine plane. The pyrazine geometry within all supramolecular calculations was not held fixed but was allowed to relax. We then calculated the n−π* transition energies for each of these structures and determined their shifts with respect to the calculated n−π* transition for isolated pyrazine.

As in our previous work with ethane,[1] we constructed representative configurations for pyrazine and 1, 2, 3, and 4 xenons. The high cost of these geometry optimizations limits our ability to thoroughly explore these potential surfaces; large basis sets and electron correlation are necessary to capture the dispersion forces that bind these clusters.[32,33,35−39] Structure **1** was used to construct four initial structures for geometry optimization of selected pyrazine and two-xenon configurations. Geometry optimization at the MP2/6-311++G(d,p)/aug-cc-pVTZ-PP level gave structures **2a**−**d** (Figure 4). Structure **2a** is the only one of these four in which the two xenons are on opposite sides of the pyrazine plane. Initial configurations of pyrazine and three xenons leading to optimized structures **3a**−**c** (Figure 5) were composites of **2**. Likewise, initial configurations of pyrazine and four xenons leading to optimized structures **4a**−**c** (Figure 6) were derived from **3**. Counterpoise corrections for **2**−**4** were computed postoptimization; the counterpoise method was not incorporated into the optimization routines.

There is evidence that the MP2 correlation method overestimates the binding energy for van der Waals clusters and that the CCSD(T) method may be necessary if accurate energies are needed.[35] We judge that high-level ab initio computations involving CCSD(T) methods are not necessary for present purposes. We need reasonable structures for the series pyrazine and 1, 2, 3, and 4 xenons at reasonable computational cost. Optimization with the 6-311++G(d,p) (C, H, N) and aug-cc-pVTZ-PP (Xe) basis sets, with diffuse functions on heavy atoms and hydrogen, satisfies this need.

Gradient optimization performed with the counterpoise (CP) correction incorporated into the routine and gradient optimization performed with the CP correction applied a posteriori (as is usually done) lead to two different potential energy surfaces; we denote these as CP-corrected and standard potential energy surfaces, respectively.[32,33] For a two-component system, each step in a gradient optimization with CP requires five separate energy calculations rather than the single calculation required

TABLE 2: Comparison of CP-Corrected and Standard Potential Energy Surfaces for the System 1, Pyrazine, and One Xenon

entry	basis set	CP[a]	$E_{corrected}$ (au)[b]	E_b (kcal)[c]	plane−Xe distance (Å)	n−π* (cm^{-1})	shift (cm^{-1})[d]
1	6-311++G(d,p) (C, H, N) aug-cc-pVTZ-PP (Xe)	no	−592.1825174	−1.58	3.572	32028.7	−94.6
2	6-311++G(d,p) (C, H, N) aug-cc-pVTZ-PP (Xe)	yes	−592.1827693	−1.74	3.772	32063.6	−59.7
3	aug-cc-pVTZ-PP (C, H, N, Xe)	no	−592.3594094	−2.18	3.479	32018.4	−101.9
4	aug-cc-pVTZ-PP (C, H, N, Xe)	yes	−592.3597067	−2.36	3.650	32046.2	−74.1
5	aug-cc-pVQZ-PP (C, N, H, Xe)[e]		−592.5445818	−2.41	3.772		
6	aug-cc-pVQZ-PP (C, N, H, Xe)[f]		−592.5449595	−2.50	3.650		

[a] Optimized on CP-corrected potential surface is "yes"; optimized on standard potential surface and corrected a posteriori is "no". [b] Counterpoise-corrected energy. [c] Cluster binding energy (mol^{-1}) relative to isolated pyrazine and xenon. [d] Entries 3 and 4 calculated with respect to transition energy (32 120.3 cm^{-1}) for isolated pyrazine geometry optimized at the MP2/aug-cc-pVTZ level. [e] Entry 5 is a single-point, CP-corrected calculation with large basis set at geometry obtained from optimization in table entry 2. [f] Entry 6 is a single-point, CP-corrected calculation with large basis set at geometry obtained from optimization in table entry 4.

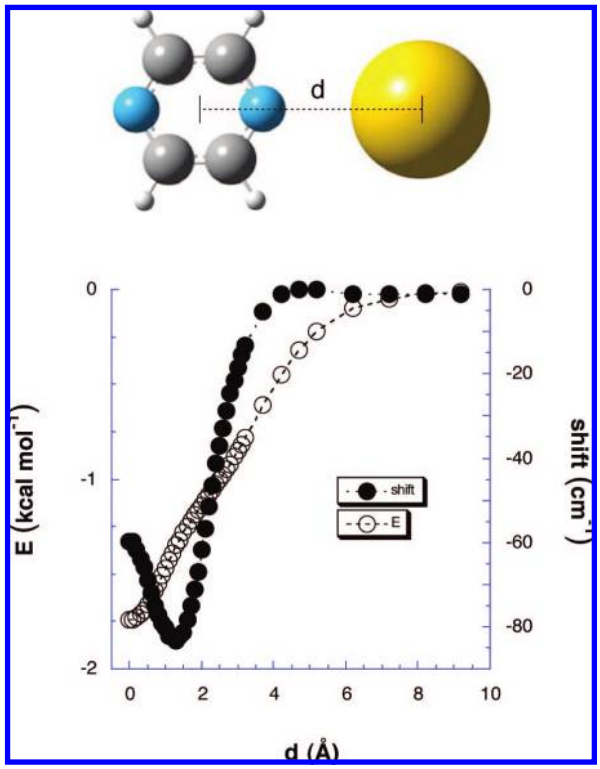

Figure 9. Energy and calculated n−π* shift of **1** as a function of xenon movement in the plane above pyrazine. Zero on the distance coordinate (d) corresponds to the potential minimum for the system. The distance coordinate is a line parallel to and 3.772 Å from the pyrazine plane. Open circles indicate the CP-corrected energy of the system as a function of distance. Filled circles indicate shift in calculated n−π* transition relative to isolated pyrazine for each of these configurations.

TABLE 3: Predicted Experimental ρ_{bulk} at 293.2 and 333.3 K for average n = 1, 2, 3, and 4 Nearest-Neighbor Xenons As Measured by Pyrazine n−π* Electronic Transition

		predicted ρ_{bulk} (g cm^{-3})	
average nXe	$\Delta\nu$ (cm^{-1})	293.2 K	333.2 K
1	−66.5	0.50	0.65
2	−133.0	0.91	1.20
3	−199.5	1.85	1.85
4	−266.0	2.50	2.50

in the absence of CP. Gradient optimizations with CP incorporated into the routine are therefore more expensive than those without CP, and there is evidence that the properties of the two surfaces may differ significantly. For example, intermolecular distances on the CP-corrected surfaces are consistently greater (about 0.1 Å or more) than those on standard surfaces.[32]

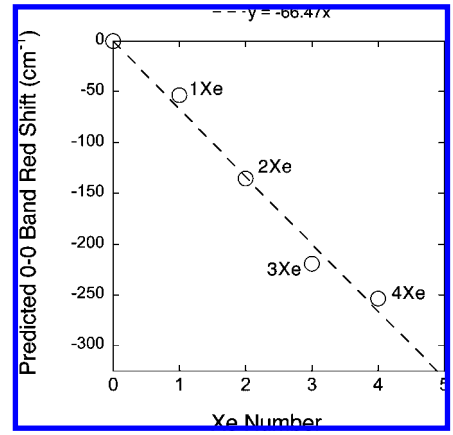

Figure 10. Red shift in pyrazine n−π* transition as a function of xenon number in pyrazine primary solvation sphere.

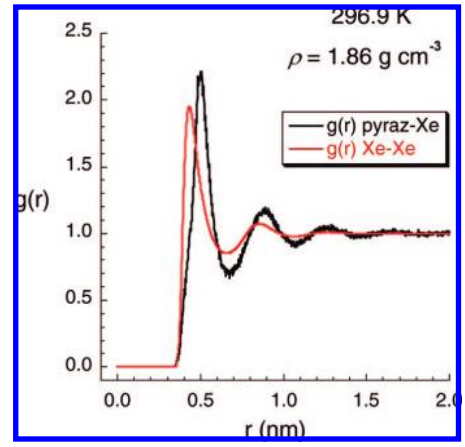

Figure 11. Radial distribution functions for pyrazine−xenon (black curve, maximum at 0.499 nm) and xenon−xenon (red curve, maximum at 0.434 nm) at the simulated 296.9 K and bulk density (1.86 g cm^{-3}) at which three xenons are predicted to lie within 5 Å of the pyrazine center of mass.

Table 2 summarizes our comparison of the CP-corrected and standard surfaces for **1**, the pyrazine, and one xenon system. Entries 1 and 2 are the geometry optimization results obtained from the same basis set for the standard and CP-corrected surfaces, respectively. The CP-corrected structure has a greater binding energy and a pyrazine−xenon distance that is 0.2 Å longer. Similarly, entries 3 and 4 are the geometry optimization results obtained from identical (but larger than for entries 1 and 2) basis sets. Again, the CP-corrected structure has a greater binding energy and a pyrazine−xenon distance that is 0.17 Å longer. The consequences of surface choice are also reflected in the calculated shifts; the magnitude of the shift is smaller for the CP-corrected surface than for the standard surface.

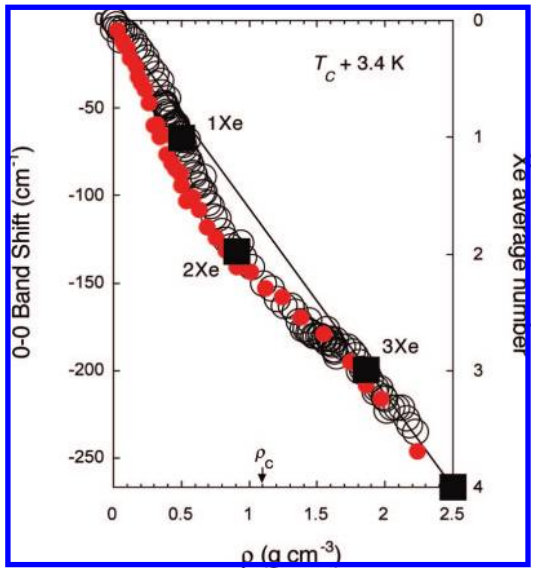

Figure 12. Superimposed: (a) experimental shift of pyrazine n−π* transition 0−0 band maximum as a function of xenon bulk density at 293.2 K (open black circles); (b) quantum chemically obtained bulk density predictions for average of 1, 2, 3, and 4 xenons in pyrazine primary solvation sphere (filled black squares); (c) molecular dynamics derived average xenon number density within 5 Å of pyrazine center of mass as a function of bulk xenon simulation density at T_C + 3.4 K (filled red circles). The line is determined by the apparently linear regions at low and high density.

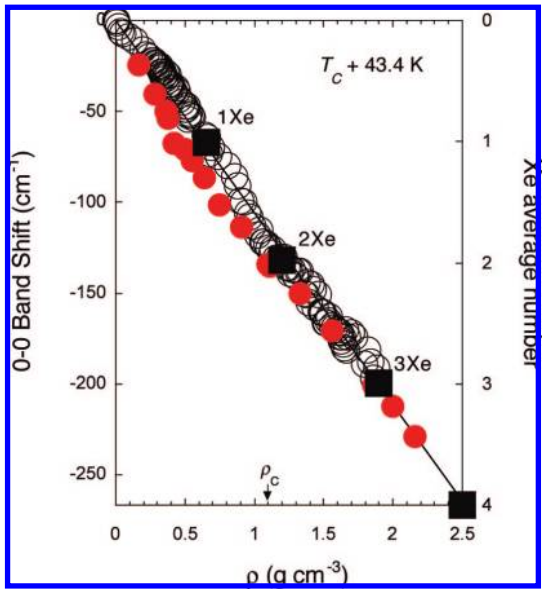

Figure 13. Superimposed: (a) experimental shift of pyrazine n−π* transition 0−0 band maximum as a function of xenon bulk density at 333.2 K (open black circles); (b) quantum chemically obtained bulk density predictions for average of 1, 2, 3, and 4 xenons in pyrazine primary solvation sphere (filled black squares); (c) molecular dynamics derived average xenon number density within 5 Å of pyrazine center of mass as a function of bulk xenon simulation density at T_C + 43.4 K (filled red circles). The line is determined by the apparently linear regions at low and high density.

Furthermore, as expected, the binding energy increases with basis set size because we have not yet reached the basis set limit. Our small sample also indicates that intermolecular distance decreases with basis set size. Finally, entries 5 and 6 are single-point, counterpoise-corrected energies calculated with the large aug-cc-pVQZ-PP basis set for the geometries in entries 2 and 4. They provide some insight into how far removed these geometries may be from those obtained by optimization at the basis set limit.

The structure denoted by entry 2 is our working structure for system **1**. All other structures reported in Table 1 for **2**, **3**, and **4** are those obtained from standard potential surfaces in which the counterpoise correction is applied only to the final, optimized structures. Frequency calculations at the MP2/6-311++G(d,p)/aug-cc-pVTZ-PP level for **1** (Table 2, entry 2) and isolated pyrazine and xenon gave vibrational zero-point energies (ZPE) of 47.86, 47.78, and 0 kcal mol^{-1}, respectively. The change in ZPE on formation of **1** (ΔZPE) is therefore 0.08 kcal mol^{-1}. This gives an estimated $\Delta H°$ of formation for **1** of −1.66 kcal mol^{-1}. The frequency calculation for **1** also allowed identification of a low-frequency vibrational mode (39.608 cm^{-1}) that corresponds to a pyrazine−xenon intermolecular stretching vibration.

Table 1 also gives our results for isolated pyrazine and xenon as well as for the xenon dimer. As previously reported,[1] calculated pyrazine bond lengths were 1.342 95, 1.394 43, and 1.087 86 Å for C−N, C−C, and C−H, respectively. Pyrazine bond lengths within the supramolecular structures **1**−**4** changed by no more than about 0.005 Å. We report the binding energies for structures **1**−**4**, obtained by subtracting the energies of the isolated species from the total energies of the structures **1**−**4**. A plot of binding energy as a function of xenon number (not shown) gives good linear correlation (R^2 = 0.998). In fact, the binding energy (E_b) as a function of xenon number (n) is reasonably represented by the expression $E_b = -1.51n$ kcal mol^{-1}. The xenon dimer (two xenon) entry agrees rather well with the experimental values[50,51] for binding energy (−0.5295 kcal mol^{-1}) and internuclear distance (4.361 Å) and is tabulated here as a point of reference. Our calculated Xe−Xe internuclear distance is 4.4424 Å at the MP2/aug-cc-pVTZ-PP level, geometry optimized on the CP-corrected surface.

Calculation of n−π* Transition. Weber and Reimers[10] showed that the TDDFT/B3LYP/cc-pVDZ method reliably gives an n−π* transition energy of 3.99 eV for pyrazine. In our hands, this method with the DGDZVP basis set, chosen because it is also defined for xenon, gave 3.980 eV (311.52 nm, 32 100.6 cm^{-1}, see below) for isolated pyrazine. These values represent average absorption frequencies and may be compared to the 3.97 eV experimental value,[10] which is the sum of the 0−0 transition energy (3.83 eV, 323.82 nm) and the estimated reorganization energy (0.14 eV).[12] We applied this method to the pyrazine and xenon structures **1**−**4** and obtained the results also tabulated in Table 1. Tabulated shifts for **2**, **3**, and **4** are Boltzmann-weighted averages of the shifts for the configurations reported in the same table and depicted in Figures 4−6. The tabulated shift for **1** is a Boltzmann-weighted average (T = 293.15 K) for all 140 configurations explored on the potential surface defined by Figures 7−9. The isolated pyrazine reference value for this shift (Table 1, 3.983 eV, 311.30 nm, 32 123.4 cm^{-1}) is obtained from structure **1** (Table 2, entry 2), from which the xenon atom has been deleted. The resultant isolated pyrazine is nearly identical to pyrazine optimized in the absence of a single xenon (ΔE_{MP2} = 0.0003 kcal mol^{-1}) and is used as the reference for construction of the potential energy surface defined by Figures 7−9. This is a compromise; otherwise, it would be necessary to geometry optimize the pyrazine component of each configuration (140 total) used to construct Figures 7−9. Our −52.8 cm^{-1} Boltzmann average shift for **1** is close to the −67 cm^{-1} shift observed by two-color double-resonance spectroscopy for the pyrazine−one xenon cluster produced by supersonic jet

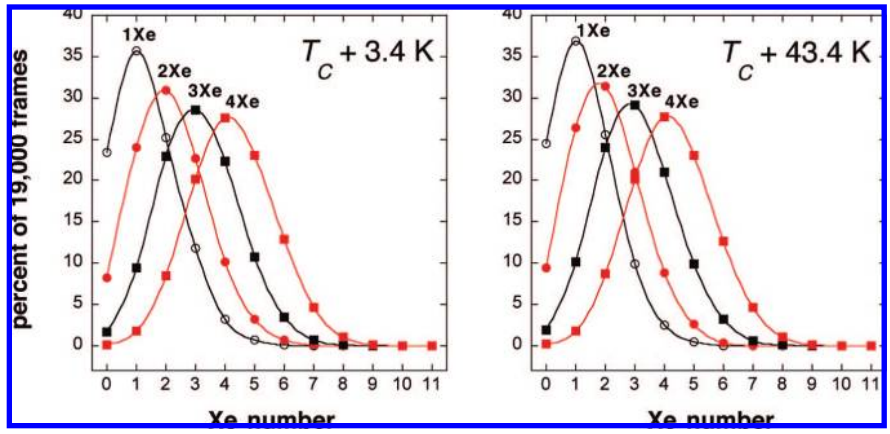

Figure 14. Xenon number density distribution within 5 Å of the pyrazine center of mass derived from molecular dynamics simulations. Left: results for T_C + 3.4 K at the predicted bulk densities for which the pyrazine primary solvation sphere is expected to be occupied by an average of 1 Xe (open circles, ρ = 0.50 g cm^{-3}), 2 Xe (red filled circles, ρ = 0.91 g cm^{-3}), 3 Xe (black filled squares, ρ = 1.85 g cm^{-3}), and 4 Xe (red filled squares, ρ = 2.50 g cm^{-3}). Right: results for T_C + 43.4 K at the predicted bulk densities for which the pyrazine primary solvation sphere is expected to be occupied by an average of 1 Xe (open circles, ρ = 0.65 g cm^{-3}), 2 Xe (red filled circles, ρ = 1.20 g cm^{-3}), 3 Xe (black filled squares, ρ = 1.85 g cm^{-3}), and 4 Xe (red filled squares, ρ = 2.50 g cm^{-3}).

expansion.[16] The validity of our geometry optimization and excited-state computational methods is thereby supported by experiment.

Probe of Structure 1 Potential Surface. The plots of xenon movement with respect to pyrazine depicted in Figures 7−9 show that the pyrazine−xenon potential surface is rather shallow. After determining the apparent global minimum at the MP2/6-311++G(d,p)/aug-cc-pVTZ-PP level for structure **1** on the CP-corrected surface, it is straightforward to construct the potential curve (Figure 7) that describes E_b as a function of perpendicular distance from xenon to the pyrazine plane. The two remaining plots in Figures 8 and 9 confine the xenon atom to a plane parallel to the pyrazine plane at the potential minimum distance (3.772 Å). Figure 8 shows E_b as a function of xenon movement in the plane that bisects the pyrazine C−C bond. Figure 9 shows E_b as a function of xenon movement in the plane that contains the pyrazine N−N axis. This attractive potential well extends to about 7 Å in the three explored dimensions.

Figures 7−9 also show our TDDFT/B3LYP/DGDZVP results, in terms of calculated n−π* transition shift relative to isolated pyrazine, for each structure obtained by variation in three dimensions. We thereby probed the sensitivity of the shift to change in location within the potential well. Compression of the intermolecular distance (Figure 7) from the potential minimum to the point at which the interaction becomes repulsive nearly quadruples the magnitude of the red shift. Increase in the intermolecular distance from the potential minimum at 3.772 Å to 5.0 Å results in a rapid decline in magnitude of the red shift to near zero. Movement of xenon in the 3.772 Å plane toward the C−C bond gives a rapid shift to the blue (maximum about +25 cm^{-1}), which declines symmetrically to zero as the xenon atom moves beyond the C−C bond. Movement of xenon in the 3.772 Å plane toward the nitrogen with its in-plane lone pair gives a rapid shift to the red (maximum about −85 cm^{-1}), which declines symmetrically to zero as the xenon atom moves beyond the nitrogen atom. Furthermore, Figures 7−9 reveal that the shift is essentially zero when xenon is 5 Å (average shift = −2.6 cm^{-1}) or more from the pyrazine center of mass. This suggests that the experimental observable is insensitive to xenon atoms beyond this distance. Our pyrazine primary solvation sphere therefore has a radius of 5 Å and is centered at the pyrazine center of mass.

Predictions. The calculated shifts for **1**−**4** show good linear correlation (R^2 = 0.984) when plotted as a function of xenon number (Figure 10). If the fit is forced to include zero, the shift ($\Delta\nu$) as a function of xenon number (n) appears additive and is reasonably represented by $\Delta\nu = -66.5n$ cm^{-1}. This estimate may better "average out" the geometry-specific shifts that are a consequence of our limited sampling of pyrazine−xenon structures. Expected shifts are therefore −66.5, −133.0, −199.5, and −266.0 cm^{-1} for n = 1, 2, 3, and 4 xenons. Visually superposing these calculated shifts for **1**−**4** on the experimental shift versus bulk density curves for 293.2 and 333.2 K (Figure 2) and then reading the corresponding bulk densities from the curves provides our graphical predictions for the bulk densities at which we expect pyrazine's nearest neighbors to average 1, 2, 3, and 4 xenons at the two temperatures (Table 3).

Evaluation of Predictions. X-ray scattering techniques would seem to hold the most promise for measurement of solvent−solute cluster size in supercritical fluids. Yonker studied the fluid structure of pure supercritical xenon by nuclear magnetic resonance (NMR) spectroscopy and small-angle X-ray scattering (SAXS) and obtained detailed information about correlation lengths and density fluctuations.[52] Nishikawa recently examined supercritical xenon density fluctuations with a new variable-path-length sample holder for SAXS measurements of samples with large mass absorption coefficients.[53] Formisano studied two- and three-body long-range forces in xenon by small-angle neutron scattering (SANS).[54] NMR can provide a rough estimate of reverse micelle diameter on the order of 10 nm in supercritical xenon.[55] Both SANS and SAXS are suitable for the study of the size and shape of supramolecular structures in supercritical media with 5−2000 Å resolution. We cannot evaluate our predictions for pyrazine in xenon with these methods because the spatial resolution is inadequate.

X-ray absorption fine-structure (XAFS) spectroscopy is a technique for investigating the local structure around a specific atom.[56] Hayakawa used Br K-edge XAFS spectroscopy to focus on the Br−Xe interaction for 1-bromonapthalene in xenon.[57] Detailed X-ray absorption near-edge structure (XANES) analyses suggested that six xenons lie within 4.85 Å of the bromine nucleus under their conditions; they did not examine the locations of xenon atoms with respect to the anthracene portion of the molecule. As the absorption coefficient for this process is directly proportional to the product of sample density and atomic number to the fourth power, detection of low atomic number atoms such as C and N of pyrazine in xenon at high dilution may not be straightforward.

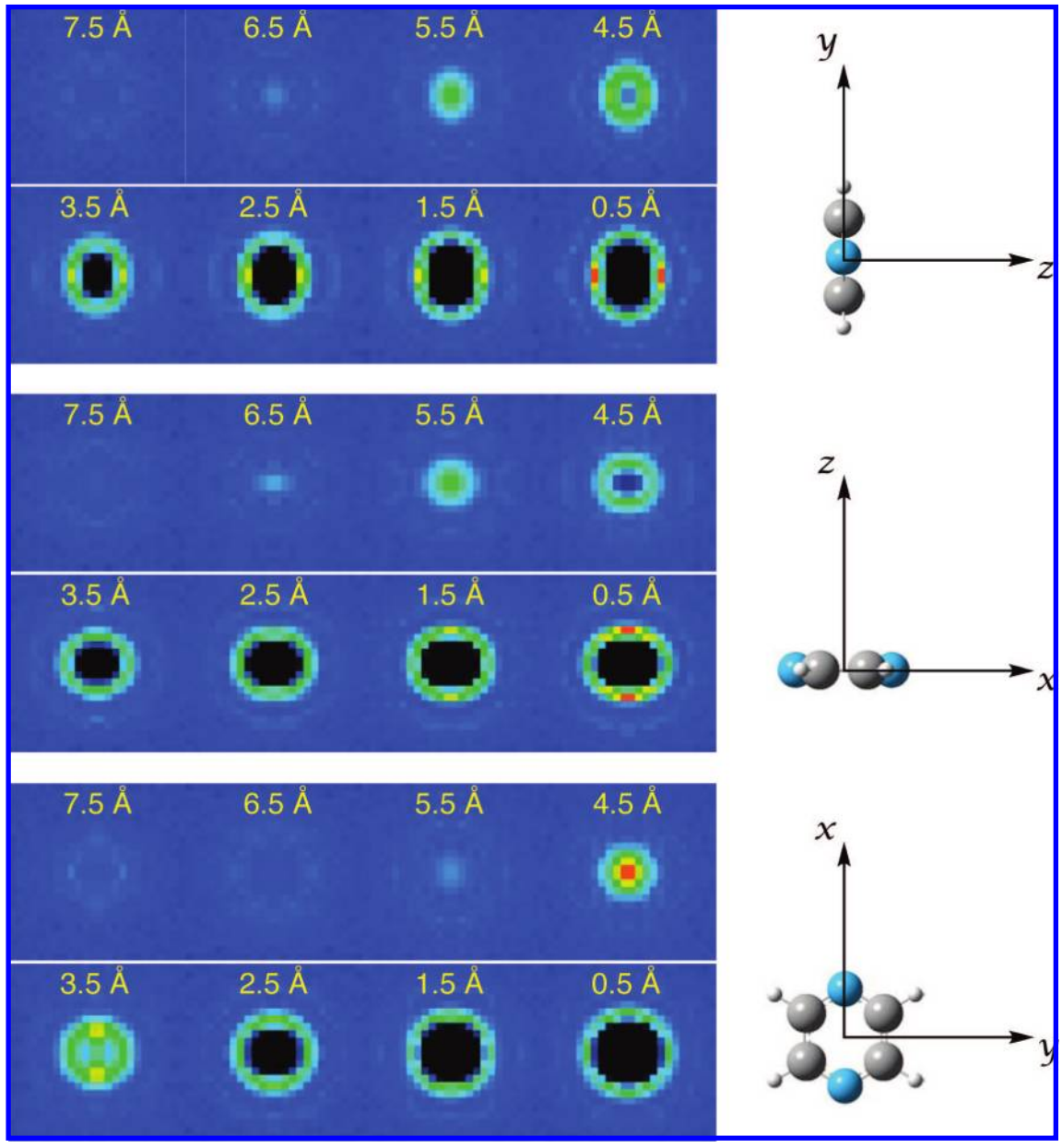

Figure 15. Probability distribution of xenon at pyrazine for simulated $T_C + 3.4$ K and xenon bulk density 0.50 g cm^{-3}. Three projections of x, y, and z axes with respect to pyrazine center of mass at the origin. Xenon probability density layers of 1 Å thickness, centered at 7.5, 6.5, 5.5, 4.5, 3.5, 2.5, 1.5, and 0.5 Å. Each layer is 25 Å square. Red is the highest xenon probability density. Top: x-projection. Middle: y-projection. Bottom: z-projection.

At present, the best way to evaluate our predictions is with classical molecular dynamics simulation.[58,59] We first verified the suitability of the Lennard-Jones potential for the united atom pyrazine−xenon interaction with a simulated annealing experiment from 300 to 1 K for pyrazine and one xenon. The resultant global minimum at about 1 K for our system is nearly identical to our quantum chemically obtained structure **1**, in which the xenon atom is poised above the pyrazine plane with C_{2v} symmetry. The distance between the xenon nucleus and the pyrazine plane is 3.98 Å in the molecular dynamics system, which compares well with our quantum chemically determined "working" structure for **1**, in which this distance is 3.772 Å and the symmetry is the same. As the Lennard-Jones result is within about 5% of the quantum chemical, and our simulated T_C is within about 1% of the experimental value, we are confident that our molecular dynamics simulation of a single pyrazine in a cubic box with 1000 xenons is a reasonable approximation of reality.

We therefore used molecular dynamics to simulate the pyrazine local environment at the two experimental temperatures, $T_C + 3.4$ K and $T_C + 43.4$ K. Representatively, Figure 11 shows the radial distribution functions for pyrazine−xenon and xenon−xenon at $T_C + 3.4$ K and 1.86 g cm^{-3} with the first maxima at $r = 0.499$ and 0.434 nm, respectively. These r values are essentially invariant with temperature and bulk density.

Quantum chemical calculation suggests that our experimental observable (UV absorbance) is unaffected by xenon atoms beyond 5 Å from the pyrazine center of mass (see Figures 7−9). We therefore determined the average number of xenons within this 5 Å primary solvation sphere for 38 simulated bulk densities at $T_C + 3.4$ K and 21 simulated bulk densities at $T_C + 43.4$ K. These average xenon numbers with respect to density (red) are plotted on the same graphs as the experimental shifts with respect to density (open circles) for $T_C + 3.4$ K and $T_C + 43.4$ K in Figures 12 and 13, respectively. These curves are nearly superimposable at both temperatures; there is a strong correlation

between simulated local number density and experimental shift as a function of bulk density. Plotted also on both graphs are the quantum chemical predictions (black squares) from Table 3 for the bulk densities at which the pyrazine primary solvation sphere is occupied by an average of $n = 1$, 2, 3, and 4 xenons. These quantum chemical predictions agree with the local xenon number densities extracted from our molecular dynamics simulations. The average xenon number within 5.0 Å of the pyrazine center of mass at the predicted densities is 1.3, 2.1, 3.0, and 4.0 at both simulation temperatures. Experiment, quantum chemical prediction, and molecular dynamics evaluation are internally consistent.

Our interest in studying solvent effects in supercritical fluids as a function of local number density and structure dictates that it is not enough that the *average* experimental, predicted, and simulated local number densities agree. The width of the average number density distribution is also important. If the distribution is narrow, the value of the technique for studying solvent effects is enhanced. Figure 14 addresses this issue. Plotted for both simulated temperatures is the percent distribution at each predicted density for 0−11 xenons. At each predicted density for $n = 1$, 2, 3, and 4 local xenons, the value for $n \pm 1$ ranges from about 85 to 71% of the total number distribution. Future use of this methodology for characterizing the local solute environment will show whether or not this distribution is narrow enough to be generally useful when studying the details of a solvent effect on a physical or chemical process.

Figure 15, derived from our molecular dynamics data, presents a qualitative, concise, color-coded way to visualize the most probable regions of space occupied by xenon with respect to pyrazine, illustrated in this case for the simulated bulk density (0.50 g cm^{-3}, T_C + 3.4 K) at which an average of one xenon is predicted to reside in the pyrazine primary solvation sphere. The axes origin is the pyrazine center of mass. Three sets of eight projections (*x*-axis onto the *yz*-plane, *y*-axis onto the *xz*-plane, and *z*-axis onto the *xy*-plane) of xenon probability are shown. Each projection is a 25 Å square slice of 1 Å thickness centered at 7.5 through 0.5 Å distance from the origin. The color black is the region of zero probability; the probability increases in the order of the colors of the visible spectrum: violet, blue, green, yellow, orange, and red. Each of the three projections shows the development of xenon order at 7.5 Å from the pyrazine center of mass. The quantum chemical exploration of the pyrazine−xenon potential surface (Figures 7−9) indicates that this is the distance at which pyrazine and xenon are beginning to feel mutual attraction. All three projections support quantum chemical structure **1** as the global minimum and also verify that the potential minimum region is fairly shallow at about 4.5 Å above the pyrazine plane. The red region of the 4.5 Å slice in the *z*-projection spans about 2 Å, and the yellow region spans about 4.5 Å. The 3.5 Å slice in the *z*-projection shows two regions (yellow) of modestly high probability not revealed by our quantum chemical probe of the surface. The centers of these two yellow regions are separated by about 6 Å, which corresponds approximately to the N−N internuclear distance (2.83 Å) plus 2 times the nitrogen van der Waals radius (2 × 1.55 Å). The nitrogen lone pairs are likely to play a role in the dispersion interaction with xenon.

Conclusion

We predict supercritical xenon bulk densities at which the pyrazine primary solvation sphere is populated by an average of 1, 2, 3, and 4 xenons using a combined experimental and quantum chemical approach. Low-temperature supersonic expansion data for the pyrazine−xenon cluster ($n = 1$) supports our quantum chemical predictions for shift as a function of cluster size.[16] Molecular dynamics simulations confirm our bulk density predictions. Simulations also afford information on the width of these average number density predictions.

The agreement between the structures for pyrazine with one xenon (**1**, Figure 3) obtained from quantum chemical geometry optimization and a molecular dynamics simulated annealing experiment might suggest that expensive quantum chemical geometry optimization is not essential. However, optimization of **1** and the subsequent computational probe of the potential surface (Figures 7−9) gave the essential pyrazine primary solvation sphere cutoff value (5.0 Å radius) most appropriate for modeling the experimental n−π^* electronic transition. It is likely that future work will involve similar optimization and potential surface probes, especially when we experimentally and theoretically examine the more complicated solvent molecules such as carbon dioxide and trifluoromethane. We do not yet know whether or not it will be generally necessary to include the counterpoise method in the optimization routine.

This combined experimental, quantum chemical, and molecular dynamics approach to characterize the local solvent number density and probable structure at a solute in supercritical fluids may prove general. If so, it can be applied to test systems that might include unimolecular photochemical reactions. Detailed knowledge of the local environment may allow us to predict the fate of an excited-state species or perhaps the probability of its formation. Such predictions based on our combined approach will be a more stringent test of its usefulness. The ultimate goal is to use supercritical fluids as tools to understand solvent effects; the present work is the foundation for that goal.

Acknowledgment. We are especially grateful to Provost M. Lowengrub and Yeshiva University for generous support of this work. We acknowledge partial support of this research through the Dr. Bernard W. Gamson Computational Science Center at Yeshiva College. We are also grateful to Ann Rae Jonas for her careful reading of this manuscript.

References and Notes

(1) Hrnjez, B. J.; Sultan, S. T.; Natanov, G. R.; Kastner, D. B.; Rosman, M. R. *J. Phys. Chem. A* **2005**, *109*, 10222–10231.
(2) Hrnjez, B. J.; Mehta, A. J.; Fox, M. A.; Johnston, K. P. *J. Am. Chem. Soc.* **1989**, *111*, 2662–2666.
(3) Reichardt, C. *Solvents and Solvent Effects in Organic Chemistry*, 3rd ed.; Wiley-VCH: Wenheim, 2003.
(4) Tucker, S. C. *Chem. Rev.* **1999**, *99*, 391–418.
(5) Kajimoto, O. *Chem. Rev.* **1999**, *99*, 355–389.
(6) Egorov, S. A. *J. Chem. Phys.* **2000**, *112*, 7138–7146.
(7) Egorov, S. A. *J. Chem. Phys.* **2000**, *113*, 1950–1957.
(8) Egorov, S. A. *J. Chem. Phys.* **2002**, *116*, 2004–2010.
(9) Egorov, S. A. *Chem. Phys. Lett.* **2002**, *354*, 140–147.
(10) Weber, P.; Reimers, J. R. *J. Phys. Chem. A* **1999**, *103*, 9821–9829.
(11) Cradock, S.; Liescheski, P. B.; Rankin, D. W. H.; Robertson, H. E. *J. Am. Chem. Soc.* **1988**, *110*, 2758–2763.
(12) Baba, H.; Goodman, L.; Valenti, P. C. *J. Am. Chem. Soc.* **1966**, *88*, 5410–5415.
(13) Bolovinos, A.; Tsekeris, P.; Philis, J. P.; Pantos, E.; ritsopoulos, G. *J. Mol. Spectrosc.* **1984**, *103*, 240–256.
(14) Innes, K. K.; Ross, I. G.; Moomaw, W. R. *J. Mol. Spectrosc.* **1988**, *132*, 492–544.
(15) Wanna, J.; Bernstein, E. R. *J. Chem. Phys.* **1986**, *84*, 927–935.
(16) Fujii, A.; Kitamura, Y.; Mikami, N. *J. Chem. Phys.* **2000**, *113*, 8000–8008.
(17) Holroyd, R. A.; Press, J. M.; Nishikawa, M.; Itoh, K. *J. Phys. Chem. B* **2007**, *111*, 6684–6689.
(18) Hill, P. A.; Wei, Q.; Eckenhoff, R. G.; Dmochowski, I. J. *J. Am. Chem. Soc.* **2007**, *129*, 962–963.
(19) Friend, D. G.; Ingram, H.; Ely, J. F. *J. Phys. Chem. Ref. Data* **1991**, *20*, 275–347.
(20) See: http://webbook.nist.gov/chemistry/.

(21) Schmidt, M. W.; Baldridge, K. K.; Boatz, J. A.; Elbert, S. T.; Gordon, M. S.; Jensen, J. H.; Koseki, S.; Matsunaga, N.; Nguyen, K. A.; Su, S. J.; Windus, T. L.; Dupuis, M.; J. A.; Montgomery, J. A. *J. Comput. Chem.* **1993**, *14*, 1347–1363.

(22) Gordon, M. S.; Schmidt, M. W. Advances in Electronic Structure Theory: GAMESS a Decade Later. In *Theory and Applications of Computational Chemistry*; Dykstra, C. E., Frenking, G., Kim, K. S., Scuseria, G. E., Eds.; Elsevier: Amsterdam, 2005.

(23) Granovsky, A. A. PC GAMESS version 7.1; http://classic-.chem.msu.su/gran/gamess/index.html.

(24) Gaussian 03, Revision C.02: Frisch, M. J.; Trucks, G. W.; Schlegel, H. B.; Scuseria, G. E.; Robb, M. A.; Cheeseman, J. R.; Montgomery, Jr., J. A.; Vreven, T.; Kudin, K. N.; Burant, J. C.; Millam, J. M.; Iyengar, S. S.; Tomasi, J.; Barone, V.; Mennucci, B.; Cossi, M.; Scalmani, G.; Rega, N.; Petersson, G. A.; Nakatsuji, H.; Hada, M.; Ehara, M.; Toyota, K.; Fukuda, R.; Hasegawa, J.; Ishida, M.; Nakajima, T.; Honda, Y.; Kitao, O.; Nakai, H.; Klene, M.; Li, X.; Knox, J. E.; Hratchian, H. P.; Cross, J. B.; Bakken, V.; Adamo, C.; Jaramillo, J.; Gomperts, R.; Stratmann, R. E.; Yazyev, O.; Austin, A. J.; Cammi, R.; Pomelli, C.; Ochterski, J. W.; Ayala, P. Y.; Morokuma, K.; Voth, G. A.; Salvador, P.; Dannenberg, J. J.; Zakrzewski, V. G.; Dapprich, S.; Daniels, A. D.; Strain, M. C.; Farkas, O.; Malick, D. K.; Rabuck, A. D.; Raghavachari, K.; Foresman, J. B.; Ortiz, J. V.; Cui, Q.; Baboul, A. G.; Clifford, S.; Cioslowski, J.; Stefanov, B. B.; Liu, G.; Liashenko, A.; Piskorz, P.; Komaromi, I.; Martin, R. L.; Fox, D. J.; Keith, T.; Al-Laham, M. A.; Peng, C. Y.; Nanayakkara, A.; Challacombe, M.; Gill, P. M. W.; Johnson, B.; Chen, W.; Wong, M. W.; Gonzalez, C.; Pople, J. A. Gaussian, Inc., Wallingford, CT, 2004.

(25) Møller, C.; Plesset, M. S. *Phys. Rev.* **1934**, *46*, 618–622.

(26) Clark, T.; Chandrasekhar, J.; Spitznagel, G. W.; Schleyer, P. v. R. *J. Comput. Chem.* **1983**, *4*, 294–301.

(27) Peterson, K. A.; Figgen, D.; Goll, E.; Stoll, H.; Dolg, M. *J. Chem. Phys.* **2003**, *119*, 11113–11123.

(28) Bauernschmitt, R.; Ahlrichs, R. *Chem. Phys. Lett.* **1996**, *256*, 454–464.

(29) Becke, A. D. *J. Chem. Phys.* **1993**, *98*, 5648–5652.

(30) Godbout, N.; Salahub, D. R.; Andzelm, J.; Wimmer, E. *Can. J. Chem.* **1992**, *70*, 560–571.

(31) Boys, S. F.; Bernardi, F. *Mol. Phys.* **1970**, 553–561.

(32) Hobza, P.; Havlas, Z. *Theor. Chem. Acc.* **1998**, *99*, 372–377.

(33) Asturiol, D.; Duran, M.; Salvador, P. *J. Chem. Phys.* **2008**, *128*, 144108(1)144108(5) .

(34) Dunning, T. H., Jr. *J. Chem. Phys.* **1989**, *90*, 1007–1023.

(35) Dunning, T. H., Jr. *J. Phys. Chem. A* **2000**, *104*, 9062–9080.

(36) Hobza, P.; Bludsky, O.; Selzle, H. L.; Schlag, E. W. *J. Chem. Phys.* **1992**, *97*, 335–340.

(37) Podeszwa, R.; Szalewicz, K. *Chem. Phys. Lett.* **2005**, 488–493.

(38) Bytautas, L.; Ruedenberg, K. *J. Chem. Phys.* **2008**, 214308(1)–214308(12) .

(39) Tsuzuki, S.; Honda, K.; Uchimaru, T.; Mikami, M.; Tanabe, K. *J. Am. Chem. Soc.* **2000**, *122*, 3746–3753.

(40) Kendall, R. A.; Dunning, T. H., Jr.; Harrison, R. J. *J. Chem. Phys.* **1992**, *96*, 6796–6806.

(41) Frenkel, D.; Smit, B. *Understanding Molecular Simulation*, 2nd ed.; Academic Press: San Diego, CA, 2002.

(42) Hansen, J.-P.; McDonald, I. R. *Theory of Simple Liquids*, 2nd ed.; Elsevier Academic Press: London, 1986.

(43) van der Spoel, D.; Lindahl, E.; Hess, B.; Groenhof, G.; Mark, A. E.; Berendsen, H. J. C. *J. Comput. Chem.* **2005**, *26*, 1701–1718.

(44) Egorov, S. A. *J. Chem. Phys.* **2004**, *121*, 6948–6955.

(45) Schuettelkopf, A. W.; van Aalten, D. M. F. *Acta Crystallogr.* **2004**, *D60*, 1355–1363.

(46) Dundee PRODRG2 Server, http://davapc1.bioch.dundee.ac.uk/prodrg/index.html.

(47) Myers, A. B.; Birge, R. R. *J. Chem. Phys.* **1980**, *73*, 5314–5321.

(48) Myers, A. B. *Annu. Rev. Phys. Chem.* **1998**, *49*, 267–295.

(49) Hrnjez, B. J.; Hefter, J. J.; Saperia, J. A. *Abstr. Pap. Am. Chem. Soc.* **2008**, (PHYS), 373.

(50) Freeman, D. E.; Yoshino, K.; Tanaka, Y. *J. Chem. Phys.* **1974**, *61*, 4880–4889.

(51) Barker, J. A.; Watts, R. O.; Lee, J. K.; Schafer, T. P.; Lee, Y. T. *J. Chem. Phys.* **1974**, *61*, 3081–3089.

(52) Pfund, D. M.; Zemanian, T. S.; Linehan, J. C.; Fulton, J. L.; Yonker, C. R. *J. Phys. Chem.* **1994**, *98*, 11846–11857.

(53) Tanaka, Y.; Takahishi, Y.; Morita, T.; Nishikawa, K. *Jpn. J. Appl. Phys* **2008**, *47*, 334–336.

(54) Formisano, F.; Barocchi, F.; Magli, R. *Physica B* **1998**, *241*−*243*, 958–960.

(55) Meier, M.; Fink, A.; Brunner, E. *J. Phys. Chem. B* **2005**, *109*, 3404–3498.

(56) Rehr, J. J.; Albers, R. C. *Rev. Mod. Phys.* **2000**, *72*, 621–654.

(57) Hayakawa, K.; Kato, K.; Fujikawa, T.; Murata, T.; Nakagawa, K. *Jpn. J. Appl. Phys.* **199**, *38*, 6423–6427.

(58) Ingrosso, F.; Ladanyi, B. M. *J. Phys. Chem. B* **2006**, *110*, 10120–10129.

(59) Adams, J. E. *J. Phys. Chem. B* **1998**, *102*, 7455–7461.

JP807586D